Faraday Discussions

Accepted Manuscript

This manuscript will be presented and discussed at a forthcoming Faraday Discussion meeting. All delegates can contribute to the discussion which will be included in the final volume.

Register now to attend! Full details of all upcoming meetings: http://rsc.li/fd-upcoming-meetings

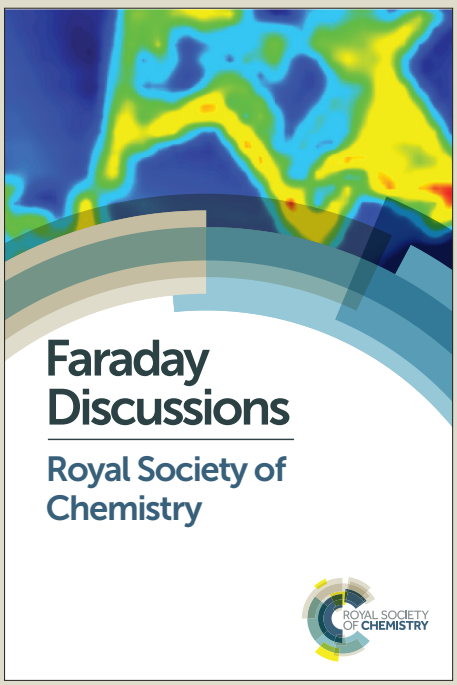

This is an *Accepted Manuscript*, which has been through the Royal Society of Chemistry peer review process and has been accepted for publication.

Accepted Manuscripts are published online shortly after acceptance, before technical editing, formatting and proof reading. Using this free service, authors can make their results available to the community, in citable form, before we publish the edited article. We will replace this *Accepted Manuscript* with the edited and formatted *Advance Article* as soon as it is available.

You can find more information about *Accepted Manuscripts* in the Information for Authors.

Please note that technical editing may introduce minor changes to the text and/or graphics, which may alter content. The journal's standard Terms & Conditions and the Ethical guidelines still apply. In no event shall the Royal Society of Chemistry be held responsible for any errors or omissions in this *Accepted Manuscript* or any consequences arising from the use of any information it contains.

ROYAL SOCIETY OF CHEMISTRY

www.rsc.org/faraday_d

A chelating diisocyanide ligand for cyclometalated Ir(III) complexes with strong and tunable luminescence

Filippo Monti,*[a] Andrea Baschieri,[b] Elia Matteucci,[b] Andrea Mazzanti,[b] Letizia Sambri,*[b] Andrea Barbieri[a] and Nicola Armaroli*[a]

DOI: 10.1039/b000000x

We report the synthesis, the structural characterisation and a detailed photophysical description of three cationic cyclometalated iridium(III) complexes (**2–4**) bearing a chelating diisocyanide as ancillary ligand (**1** = 2,2”-diisocyano-1,1’:3’,1”-terphenyl). All compounds display irreversible reduction and oxidation potentials and emit from a triplet excited state centred on the cyclometalating ligands with lifetimes of several dozens microseconds, as commonly observed for other iridium(III) isocyanide complexes and further confirmed by DFT calculations. Room-temperature photoluminescence can be tuned from blue to orange upon variation of the cyclometalating ligands and related quantum yields range from around 30% in acetonitrile solution to nearly 80% in solid-state, as for complex **3** embedded in a 1% w/w poly(methyl methacrylate) matrix.

Introduction

In recent years, the influence of supramolecular photochemistry has extended over many research fields. In some cases, light-induced properties of materials depend upon the interactions between photoactive molecular species and bulk matrices. This is the case, for instance, of dye-sensitized solar cells, which convert light energy into electricity, and electroluminescent devices, which convert electricity into light. In a broad sense, photoactive materials operating in such devices can be considered as belonging to the supramolecular photochemistry realm, since their successful functioning crucially depends on the appropriate matching between different chemical components which tightly interact.

Cyclometalated Ir(III) complexes are one of the most widely exploited classes of triplet emitters for flat solid-state electroluminescent devices such as organic light-emitting diodes (OLEDs)[1,2] and light-emitting electrochemical cells (LECs).[3,4] Key advantages of these complexes are high photoluminescence quantum yields (PLQYs), relatively short excited-state lifetimes and high versatility in tuning the

[a] *Istituto per la Sintesi Organica e la Fotoreattività, Consiglio Nazionale delle Ricerche, Via P. Gobetti 101, 40129 Bologna, Italy. Tel: +39 051 639 9820; E-mail: filippo.monti@isof.cnr.it; nicola.armaroli@isof.cnr.it*

[b] *Dipartimento di Chimica Industriale “Toso Montanari”, Università di Bologna, Viale Risorgimento 4, 40136 Bologna, Italy. Tel: +39 051 209 3614; E-mail: letizia.sambri@unibo.it*

*† Electronic Supplementary Information (ESI) available: X-ray crystallographic data of complex **3**, cyclic voltammograms of **2–4**, DFT calculated geometry of **3** both in its ground and lowest triplet excited states, emission spectra of **2–4** in solid state (PMMA matrix 1% w/w), and NMR spectra of all the reported compounds (^{1}H, ^{13}C and ^{19}F). See DOI: 10.1039/b000000x/*

emission colour by ligand variation.[3] Over the years, we have devoted substantial research effort in finding high-energy emitting cationic Ir(III) complexes for the generation of blue and white light in LECs.[5-9] Among them, cyclometalated Ir(III) complexes bearing commercially-available monodentate isocyanide ancillary ligands display the highest PLQYs (around 50-70%) and the bluest emissions (approx. 450 nm).[5-7,9-13] However, this class of compounds exhibits relatively long excited state lifetimes and low stability in LECs.[3] In order to improve these crucial features, we designed and prepared the first examples of complexes (**2–4**), bearing a remarkably large bidentate diisocyanide chelating ancillary ligand (**1**). Their structural and photophysical properties are presented herein and compared to those of analogous complexes reported in the literature.[5,7]

Results and discussion

Ligand and complex synthesis

Various luminescent cationic Ir(III) complexes containing commercially available monodentate isocyanides that serve as ancillary ligands have been reported.[5-7,9-13] These strong-field ligands contribute to increase the *d*-orbital splitting of the iridium(III) metal centre shifting the related complex emission to the blue with high photoluminescence quantum yields.[3,5,12] However these luminophores display low stability in LECs if compared to analogous complexes containing bidentate ancillary ligands, such as conventional 2,2'-bipyridines or 1,10-phenanthrolines.[3] With the aim to overcome this problem, we designed and synthesised the first example of chelating diisocyanide (**1**) that has proved successful as bidentate ligand in the preparation of three differently cyclometalated cationic Ir(III) complexes (**2–4**), which are reported in Fig. 1.

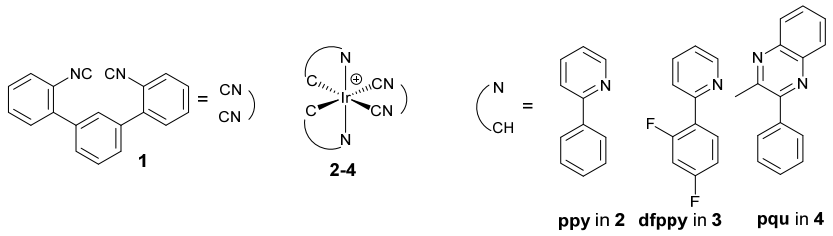

Fig. 1 Structures of ligand **1** and complexes **2–4**.

The diisocyanide ligand **1** was obtained according to the synthesis reported in Scheme 1. A Suzuki coupling between the commercially available 1,3-dibromo-benzene (**5**) and 2-aminophenylboronic acid pinacol ester gave the diamino derivative **6** in 85% yields. The treatment of **6** with ethyl formate in acetic acid at reflux resulted in the diformylated product **7** (93% yields), which was subsequently dehydrated with $POCl_3$ to give the desired ligand **1** (50% yields).

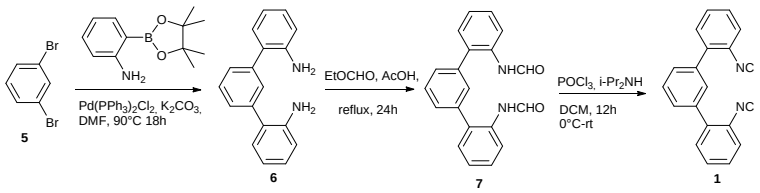

Scheme 1 Synthesis of the bidentate isocyanide ligand **1**

The diisocyanide **1** was then used as ancillary ligand to prepare the monocationic Ir(III) complexes **2–4** (Scheme 2). The cyclometalated μ-dichloro-bridged iridium precursors $[Ir(C^N)_2Cl]_2$ (**8–10**) were prepared following a reported procedure[14,15] by refluxing, in a 2-ethoxyethanol/water mixture (3:1), the $IrCl_3 \cdot xH_2O$ salt and the appropriate cyclometalating ligand HC^N, *i.e.* Hppy = 2-phenylpyridine for **8**, Hdfppy = 2-(2,4-difluoro-phenyl)pyridine) for **9**, and Hpqu = 2-methyl-3-phenylquinoxaline for **10**. Compounds **8–10** were treated with $AgBF_4$ and then, after filtration of the precipitated AgCl, ligand **1** was added to each solution and the reaction mixture was stirred at room temperature for 24 hours. Purification of the crudes by column chromatography on neutral alumina gave complexes **2–4** in good yields, (57-60%).

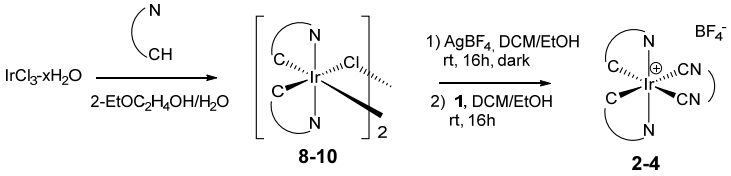

Scheme 2 Synthesis of complexes **2–4**

The treatment of **8–10** with a soluble Ag(I) salt (*i.e.*, $AgBF_4$) to remove the chloride from the dichloro-bridged dimers is an essential step for the successful accomplishment of the reaction.[16] In fact, in the absence of this step, compound **1** behaves as a monodentate ligand and coordinates two Ir(III)-fragments, both of them preserving one chloride ion in the metal coordination sphere.

Structural characterisation

The complexes **2–4** were characterized by NMR spectroscopy and ESI mass spectrometry. For all of them, the experimental molecular-ion peak pattern observed in ESI spectra is always in perfect agreement with the expected one (see Electronic Supplementary Information), exhibiting the natural isotopic abundance of the constituent elements.

The molecular structure of **3** was also determined by single-crystal X-ray diffraction analysis and is depicted in Fig. 2. Crystals were grown by slow vapor diffusion of diethyl ether into a solution of $CH_2Cl_2/CHCl_3$. The molecule crystallises in a centrosymmetric P21/n cell accommodating both the enantiomers of complex **3**. The structure was deposited with the CCDC number 1062816. Repeated attempts to obtain good single crystals of **2** and **4** were not successful.

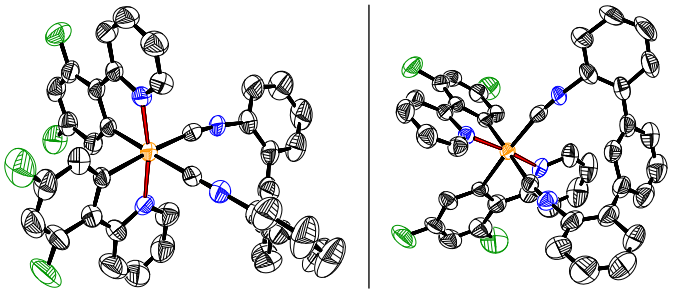

Fig. 2 X-ray crystal structure of **3** viewed from two different perspectives. The BF_4^- counteranion, solvent molecules and hydrogen atoms are omitted for clarity. ORTEP representations are at the 50% probability.

Complex **3** displays a distorted octahedral geometry, with the two pyridyl moieties of the C^N ligands mutually in *trans* position, as often observed for similar cationic cyclometalated iridium(III) complexes.[2,3] The C^N bite angles are 79° and 80°, while the NC–Ir–CN angle is 87.5°. The two Ir–CN distances are both 2.01 Å. The crystal cell contains also two solvent molecules (CH_2Cl_2), one of which is disordered over two positions.

As clearly visible from the crystal structure of **3** reported in Fig. 2, the ancillary ligand **1** is not planar so that the complex lacks any symmetry element other than the identity and, consequently, belongs to the C_1 point group. Accordingly, the two cyclometalating ligands are not equivalent, as confirmed by NMR spectra (see ESI). In fact, a splitting of the signal coming from the two C^N ligands is observed in the ^1H and ^{13}C NMR spectra, when the motion of the terphenyl moiety on ligand **1** is sufficiently slow with respect to the NMR timescale. The dynamic behavior of this class of compounds was confirmed in the case of **4**. At room temperature the ^1H-NMR spectrum of this complex shows broad signals that can be resolved into pairs by lowering the temperature to –10°C (see ESI for the NMR spectra at different temperatures).

Electrochemical properties

The electrochemical properties of complexes **2–4** were investigated by Osteryoung square-wave voltammetry (OSWV) and cyclic voltammetry (CV). All the experiments were carried out in room-temperature acetonitrile solutions and reported relative to the Fc^+/Fc redox couple (see Experimental section for further details). Redox potentials for all the complexes are collected in Table 1 and compared with DFT data (*vide infra*), while the voltammograms are reported in Fig. 3 and Fig. S1. All the observed redox processes were irreversible at any scan rate (100–2000 mV s^{-1}, Fig. S2) as commonly observed for iridium(III) isocyanide complexes.[5-7]

Table 1 Electrochemical data of **2–4** determined by OSWV in room-temperature acetonitrile solution + 0.1 M $TBAPF_6$. Ferrocene is used as internal reference. Experimental data are also compared with HOMO and LUMO energy levels calculated by DFT.

Complex	Electrochemical data[a] [V]			DFT calculated energy[c] [eV]		
	E_{ox}	E_{red}	ΔE_{redox}[b]	E_{HOMO}	E_{LUMO}	ΔE_{DFT}[d]
$[Ir(ppy)_2(bpy)]^+$	+0.84[e]	–1.77,[e] –2.60[e]	2.61	–5.86	–2.28	3.58
2	+1.23	–2.29, –2.53	3.52	–6.46	–1.77	4.69
3	+1.60	–2.18, –2.42	4.02	–6.70	–1.85	4.85
4	+1.30	–1.42, –1.73	2.72	–6.62	–2.75	3.87

[a] All redox processes were irreversible. Estimated errors: ± 50 mV. [b] $\Delta E_{redox} = E_{ox} - E_{red}$. [c] DFT calculations were carried out at the M06/6-31G(d,p)&LANL2DZ(Ir) level of theory in acetonitrile, using PCM. [d] $\Delta E_{DFT} = E_{LUMO} - E_{HOMO}$. [e] Data from literature.[3]

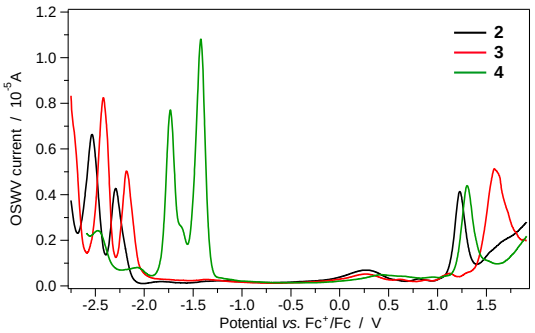

Fig. 3 Square-wave voltammograms of **2–4** in room-temperature acetonitrile solutions recorded at a scan rate of 25 mV/s with a square-wave amplitude of ±20 mV and a frequency of 25 Hz.

The first oxidation process always involves the Ir–phenyl moiety of the cyclometalating ligands.[3,5] As a consequence, the presence of the electron-withdrawing fluorines in the dfppy ligands significantly increases the oxidation potential of complex **3** by 0.37 V, if compared to **2**. This is a well-known feature for cationic Ir(III) cyclometalated complexes.[3,4] Such a halogen substitution also induces a small stabilisation of the LUMO, that results in slightly less negative reduction potentials for complex **3** with respect to the unsubstituted analogue **2** (+0.11 V). Anyway, the overall effect is an increase in the redox gap of around 0.50 V, on passing from **2** to **3**.

A very different trend is observed in the case of **4**, which displays a redox gap of only 2.72 V *vs.* 3.52 and 4.02 V for **2** and **3**, respectively. This reduced electrochemical gap should be predominantly ascribed to LUMO stabilisation due to the presence of the π-extended quinoxaline moiety on its cyclometalating ligands. In fact, the oxidation potential of this complex is comparable to that of **2** (*i.e.*, +1.30 *vs.* +1.23 V), while the reduction potential shifts positively by approx. +0.80 V. This experimental evidence suggests that the reduction processes always involve the pyridyl (or quinoxaline) moiety of the cyclometalating ligands and not the chelating isocyanide moiety, as also indicated by DFT calculations (*vide infra*). The two cathodic peaks of **4** between –1.0 and –2.0 V (Fig. 3) can be reasonably ascribed to two analogue processes involving the reduction of the first cyclometalating ligand, followed by the reduction of the second one at more negative potentials. In fact, DFT calculations indicate that both LUMO and LUMO+1 are very close in energy and centred on the same region of the two identical cyclometalating ligands (*vide*

infra).

It should also be emphasised that the electrochemical data correlate well with the theoretically calculated ones (Table 1), indicating that both methods give the same qualitative picture of the ground-state electronic properties of this class of iridium(III) complexes, as extensively discussed in the next section.

Ground-state theoretical calculations

The molecular structures and the electronic properties of complexes **2–4** were investigated by density functional theory (DFT) calculations and compared to X-ray crystallographic structures (for **3**) and electrochemical data. The M06 hybrid meta exchange-correlation functional[17,18] was used in combination with the 6-31G(d,p) basis set for all the atoms,[19] except in the case of the Ir(III) metal centre where the LANL2DZ pseudopotential and the related basis-set was selected (see Experimental section).[20] The ground-state (S_0) geometries of **2–4** were fully optimized without symmetry constraints in acetonitrile, using the polarizable continuum model (PCM).[21-23] The quality of the theoretically optimized geometries was evaluated by comparison with the available X-ray crystal structure of **3**, which can be reasonably utilized also to model **2** and **4**. In Fig. S3 the structural overlap between the X-ray crystal structure of **3** and the theoretically computed one is reported. No substantial differences are found between the two geometries, as corroborated by the low value (0.127 Å) of the minimized root-mean-square deviation (RMSD) of all the atomic positions (except hydrogen atoms). This finding proves the effectiveness of the selected computational model and indicates that strong intermolecular interactions are not present in the crystal.

The frontier molecular orbitals of **2–4** are depicted in Fig. 4. As generally found for cyclometalated cationic iridium(III) complexes, the HOMO is localized on the Ir(III) metal centre and on both the phenyl moiety of the two cyclometalating C^N ligands, while the LUMO and the LUMO+1 mainly reside on the nitrogen-containing ring of each cyclometalating ligand, as commonly observed for other iridium(III) isocyanide complexes.[3,4] The latter feature is substantially different from what is observed for the archetypal complex $[Ir(ppy)_2(bpy)]^+$, where the LUMO is located on the π* orbitals of the 2,2'-bipyridine ancillary ligand. Therefore, the chelating diisocyanide ligand **1** still exhibits relatively inaccessible π* orbitals despite its more extended π-conjugation, if compared to commercially available monodentate isocyanide ligands such as *tert*-butyl isocyanide (CN-*tert*-Bu) or 2,6-dimethylphenyl isocyanide.[5-7,12] As a consequence, the lowest unoccupied molecular orbitals centred on this ancillary ligand are the LUMO+2 and LUMO+3 for all of the three complexes.

The presence of a strong-field ligand such as **1** induces a remarkable stabilisation of the HOMO in **2–4** if compared to the archetypal $[Ir(ppy)_2(bpy)]^+$ complex (approx. –0.73 eV). This stabilisation is maximized in the case of **3** (–0.84 eV) due to the fluorine substituents on the phenyl moiety of the dfppy cyclometalating ligands.[3] On the other hand, in the case of **4**, a pronounced LUMO (and LUMO+1) stabilisation is observed due to the π-extended quinoxaline moiety on the cyclometalating ligands.

Theoretical calculations predict that the HOMO–LUMO energy gap increases along the series $[Ir(ppy)_2(bpy)]^+$ (3.58 eV) < **4** (3.87 eV) < **2** (4.69 eV) < **3** (4.85 eV). This trend is in full agreement with the electrochemical gaps obtained from OSWV measurements (Table 1).

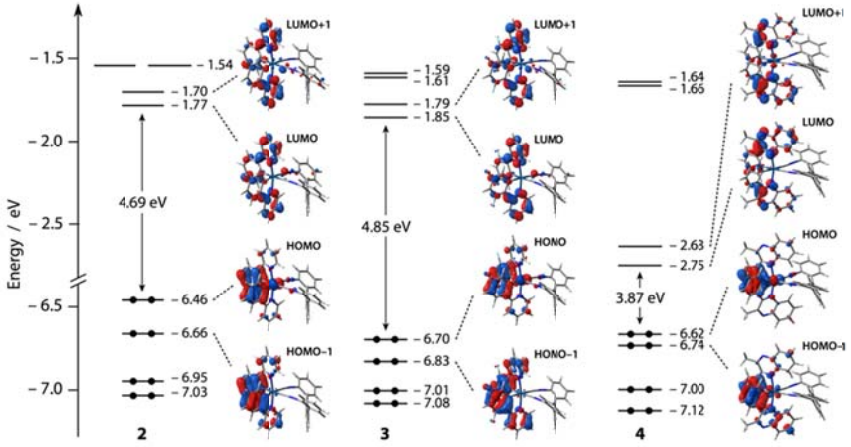

Fig. 4 Energy diagram showing the frontier Kohn–Sham molecular orbitals of complexes **2–4** in acetonitrile calculated at the PCM-M06/6-31G(d,p)&LANL2DZ(Ir) level of theory. For some relevant orbitals, the corresponding isosurface is also displayed (isovalue = 0.04 $e^{1/2}$ $bohr^{-3/2}$).

Photophysical properties and excited-state characterisation

All the complexes are stable in acetonitrile solution for several months and do not show degradation under standard laboratory conditions. The room-temperature electronic absorption spectra of **2–4** are reported in Fig. 5 and compared with the theoretically calculated ones in Figs. S4–S6.

The spectral window between 200 and 300 nm shows intense absorption bands ($\varepsilon \approx 2–10 \cdot 10^4$ M^{-1} cm^{-1}) that are assigned to spin-allowed ligand-centred (LC) π–π* transitions involving both the cyclometalating and the ancillary ligand **1**. On the other hand, the weaker bands at longer wavelength could also display a contribution from the iridium *d* orbitals and arise from transitions of both singlet and triplet spin multiplicity, due to the high spin-orbit coupling constant of the iridium metal centre.

Complex **2** is taken as representative example of the series to discuss the absorption spectra more rigorously. The lowest-energy band in the 325–375 nm region is attributed to the $S_0 \rightarrow S_1$ transition involving an almost pure HOMO→LUMO excitation (90%, Fig. 4 and Fig. S4) and is consequently LC in nature with a small metal-to-ligand charge-transfer (MLCT) contribution. It is interesting to notice that the shoulder centred at 300 nm is actually composed by a cluster of four electronic transitions (from $S_0 \rightarrow S_3$ to $S_0 \rightarrow S_6$, Fig. S4) displaying different origins. The first two excitations can be described as HOMO–1 to LUMO and LUMO+1 excitations (Fig. 4), so they are basically LC in nature and involve the phenyl-pyridine cyclometalating ligands. On the other hand, the last couple of excitations concern transitions from the HOMO to the LUMO+2 and LUMO+3 (*i.e.*, the lowest-laying π* orbitals of ligand **1**) and they are consequently MLCT in nature with a remarkable ligand-to-ligand charge-transfer (LL'CT) character.

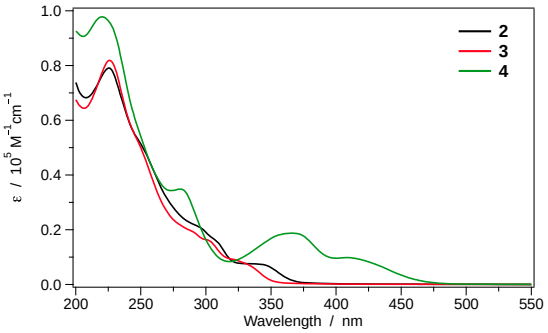

Fig. 5 Absorption spectra of **2–4** in acetonitrile solution at 298 K.

In the case of **3**, no substantial differences are observed in the absorption spectrum compared to **2**, apart from a remarkable blue shift (approx. 20 nm) of the previously described lowest-energy absorption bands due to the presence of the fluorine substituents on the cyclometalating ligands that strongly stabilize the HOMO with respect to complex **2**. This is a common feature of fluorinated cationic iridium(III) complexes and is widely described in literature.[3,4,24,25]

The absorption spectrum of complex **4** extends up to 475 nm due to the presence of the phenyl-quinoxaline cyclometalating ligands. The first four singlet transitions, contributing to the lowest-energy broad absorption band between 380 and 450 nm (Fig. 5), involve electronic excitations from the HOMO–1 and HOMO to the LUMO and LUMO+1 (Fig. 4 and Fig. S6). As a consequence, they all display a mixed MLCT/LC character. The second experimental absorption band in the 325–400 nm range (Fig. 5) can be mostly described by the $S_0 \rightarrow S_7$ and $S_0 \rightarrow S_8$ transitions that are supposed to dominate the absorption spectrum in that region, due to their large oscillator strength ($f \approx 0.16$, Fig. S6). Both excitations are almost pure LC transitions involving the promotion of one electron from the phenyl moiety of the cyclometalating ligands to their quinoxaline subunit, with virtually no contribution of the iridium *d* orbitals.

The emission spectra of **2–4** are reported in Fig. 6 both in acetonitrile solution at 298 K (full lines) and at 77 K (dashed lines), while in Table 2 are summarized the luminescence properties and photophysical parameters of all the complexes, including solid-state PMMA matrix. The room-temperature luminescence spectra of complexes **2** and **3** display a strongly pronounced vibronic structure, indicating the LC character of the emitting state, as typically observed in other isocyanide cationic iridium(III) complexes.[3,5-7,9-13] A blue shift of 0.08 eV is observed in the case of **3**, if compared to **2**, as typically detected for bis-fluorinated complexes (Fig. 6).[3,24,25] On the contrary, an orange emission is recorded for complex **4** (λ_{max} = 630 nm) and, in this case, the spectrum at 298 K is broad and unstructured with no vibronic progressions (Fig. 6).

Table 2 Luminescence properties and photophysical parameters of **2–4**.

	Oxygen-free CH_3CN solution, 298 K					Rigid matrix CH_3CN, 77 K		1% PMMA matrix, 298 K				
	λ_{em} [a] [nm]	Φ_{em} [b] [%]	τ [c] [μs]	k_r [d] [10^3 s^{-1}]	k_{nr} [e] [10^4 s^{-1}]	λ_{em} [a] [nm]	τ [c] [μs]	λ_{em} [nm]	Φ_{em} [f] [%]	τ [c] [μs]	k_r [d] [10^3 s^{-1}]	k_{nr} [e] [10^4 s^{-1}]
2	452, 483	24	27.5	8.86	2.75	465, 485, 498	6.3 (62%) 40.1 (38%)	453, 484	68	36.4	18.6	0.89
3	438, 468	37	45.0	8.27	1.40	446, 469, 477	46.5 (33%) 57.3 (67%)	440, 469	79	59.7	13.1	0.36
4	630	25	16.4	15.0	4.60	596, 633	12.7 (60%) 29.9 (40%)	618	19	19.9	9.75	4.05

[a] λ_{exc} = 325 nm; [b] λ_{exc} = 325 nm, quinine sulfate in 1 N H_2SO_4 aqueous solution as reference; [c] λ_{exc} = 370 nm; [d] $k_r = \Phi/\tau$; [e] $k_{nr} = \Phi/\tau$; [f] determined using an integrating sphere.

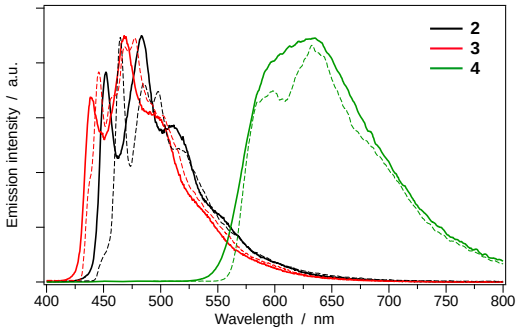

Fig. 6 Normalized emission spectra of **2–4** in acetonitrile solution at 298 K (full lines) and at 77 K (dashed lines). Excitation wavelength: 325 nm.

Anyway, also in this case, DFT calculations (*vide infra*) suggest that the emission arises from a LC triplet state centred on the 2-phenylquinoxaline cyclometalating ligands, with minimal admixture of metal-to-ligand charge-transfer character. This assumption is further corroborated by the absence of any spectral shift in the emission profile of **4** when going from room temperature to 77 K, where the only observed difference is a better spectral resolution. At low temperature, **2** and **3** again exhibit very similar behaviour.

These experimental findings are in excellent agreement with the spin-unrestricted DFT calculations carried out by fully optimizing the lowest triplet state (T_1) of **2–4**. In fact, after relaxation, the T_1 state of all the complexes preserves its ligand-centred character, as revealed by the spin-density distribution shown in Fig. 7.

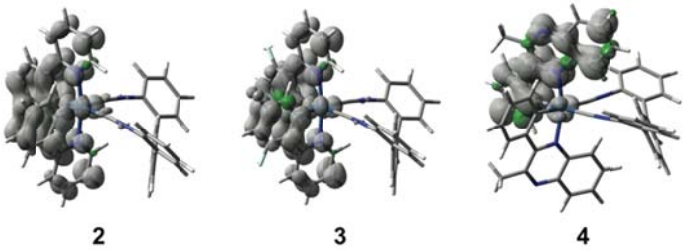

Fig. 7 Spin-density distributions calculated for the fully relaxed lowest triplet state (T_1) of complexes **2–4** in acetonitrile at the PCM-UM06/6-31G(d,p)&LANL2DZ(Ir) level of theory (surface isovalue = 0.002 e $bohr^{-3}$).

In all of the cases, the spin-density distribution matches the topology of the HOMO → LUMO excitation (Fig. 4) and confirms that the excited state is centred on the cyclometalating ligand only, without involving the chelating diisocyanide unit **1**. The calculated emission energies (see Experimental section for details) are computed to be 3.00 eV (413 nm), 3.26 eV (380 nm) and 1.79 eV (692 nm) for **2**, **3** and **4**, respectively. These values correlate well with the experimental ones (Table 2).

The photoluminescence quantum yields (PLQYs) in room-temperature acetonitrile solution of **2–4** are around 30%, the bis-fluorinated complex **3** being the strongest emitter with a PLQY of 37% (Table 2). These values are lower if compared to other iridium(III) complexes having isocyanides as ancillary ligands.[5,6,12] For instance, if complex **2** is compared to the very similar $[Ir(ppy)_2(CN\text{-}tert\text{-}Bu)_2]^+$ analogue, despite an almost superimposable emission, a 50% decrease in the PLQY is observed (*i.e.*, 24% *vs.* 52%).[5] This can be tentatively ascribed to the more "floppy" chelating ligand **1** that may promote non-radiative deactivation pathways with respect to the more rigid "rod-like" monodentate *tert*-butyl isocyanide ligand.

In Fig. S7 are reported the room-temperature emission spectra of **2–4** in the solid state, dispersed in a poly(methyl methacrylate) (PMMA) matrix at a concentration of 1% by weight. All the emission profiles are virtually superimposable with those recorded in acetonitrile solution at 298 K, suggesting that the external environment negligibly affects the ^{3}LC emitting state of these complexes. For **4**, also the PLQY and lifetime values in solid state are almost comparable with those observed in room-temperature acetonitrile, whereas the emission quantum yields of **2** and **3** in PMMA display approximately a two-fold increase, leading to the quite remarkable value of 78.5% for the fluorinated complex **3** (Table 2). Such an improvement in the emission performances of **2** and **3** can be ascribed to a three-fold decrease in the non-radiative deactivation rate constant (k_{nr}) combined by a twice as fast radiative decay rate, with respect to solution. While the former finding can be easily rationalized in the PMMA solid matrix, where the rigidity of the ligand **1** may increase, the latter observation is more difficult to explain since the nature of the excited state is expected to be the same both in acetonitrile and in PMMA matrix. Anyhow, an increase in the k_r values on passing from solution to solid state is generally observed in cationic iridium(III) complexes with cyclometalating phenylpyridines and monodentate ancillary isocyanides, so the data in Table 2 are in line with analogous complexes reported in the literature.[5,6]

Conclusions

Complexes **2–4** are the first examples of Ir(III) cationic complexes equipped with an isocyanide chelator (**1**) as ancillary ligand. HOMO and LUMO orbitals (as well as HOMO–1 and LUMO+1) of **2–4** virtually involve only the cyclometallating ligands and the iridium *d* orbitals. Therefore, **1** has a key structural role but does not affect the energy and nature of the lowest electronic excited states of the complexes, which only depend on the cyclometalating moieties. This combination of structural and electronic features enables tuning of the emission colour of **2–4** by a suitable modification of the C^N ligands, going from blue to orange upon extension of π-conjugation from phenylpyridine to phenylquinoxaline. Notably, the photoluminescence quantum yield of these very stable complexes is moderate to very high in all cases and under any experimental conditions (≈ 20–80%). This makes them very interesting candidates for optoelectronic applications and sensing.

Experimental section

General synthetic procedures

Analytical grade solvents and commercially available reagents were used as received, unless otherwise stated. Chromatographic purifications were performed using 70-230 mesh silica. Solvents were dried and distilled according to standard procedures and stored under nitrogen. ^{1}H, ^{13}C, ^{19}F NMR spectra were recorded on a Varian Inova 300 MHz, on a Mercury 400 MHz or on an Inova 600 MHz spectrometer. Chemical shifts (δ) are reported in ppm relative to residual solvent signals for ^{1}H and ^{13}C NMR (^{1}H NMR: 7.26 ppm for $CDCl_3$; ^{13}C NMR: 77.0 ppm for $CDCl_3$). ^{13}C NMR spectra were acquired with ^{1}H broadband decoupling mode. Mass spectra were recorded on a micromass LCT spectrometer using electrospray (ES) ionisation techniques.

Synthesis of the ligand (1)

(1,1':3',1''-terphenyl)-2,2''-diamine (6)

1,3-Dibromobenzene (**5**) (120.0 mg, 0.49 mmol) and 2-aminophenylboronic acid pinacol ester (440.0 mg, 2.0 mmol) were dissolved in dimethylformamide (8 mL). The resulting solution was degassed with nitrogen for 10 minutes. Then K_2CO_3 (2M in water, 2.5 mL, 5.0 mmol) was added, and the solution was degassed for additional 30 minutes. $Pd(PPh_3)_2Cl_2$ (18.0 mg, 0.05 mmol) was then added and the mixture was heated under nitrogen atmosphere at 90°C for 18 hours. After this time, water (30 mL) was added and the resulting mixture was extracted with ethyl acetate (4 x 15 mL). The collected organic phase was washed with water (30 mL) and brine (30 mL), dried over Na_2SO_4 and concentrated. The crude was purified on silica gel flash chromatography using a mixture of *n*-hexane/ethyl acetate (8:2) to give product **6** in 85% yield (108 mg).[26] ^{1}H NMR ($CDCl_3$, 300 MHz) δ 7.58-7.42 (m, 4H), 7.18-7.13 (m, 4H), 6.83 (td, J_T = 7.4, J_D = 1.2 Hz, 2H), 6.78 (dd, J = 8.3 Hz, J = 1.2 Hz, 2H), 3.81 (bs, 4H).

2,2''-diisocyano-1,1':3',1''-terphenyl (1).

[1,1':3',1''-terphenyl]-2,2''-diamine (**2**) (130.0 mg, 0.5 mmol) was dissolved in ethyl formate (921 µL, 12.5 mmol) and acetic acid (56 µL, 1.0 mmol) was added. The resulting solution was refluxed for 24 hours. The solvent was then evaporated. Water (30 mL) was added and the mixture was extracted with ethyl acetate (4 x 15 mL). The collected organic phase was washed with water (30 mL) and brine (30 mL), dried over Na_2SO_4 and concentrated to give product **7** (147 mg). The crude was used in the next step without purification. It was dissolved in dry dichloromethane (5 mL) and the solution was cooled at 0°C. Diisopropylamine (981 µL, 7.0 mmol) was added and the resulting mixture was stirred at 0°C for 15 min. Phosphorous oxychloride (137 µL, 1.5 mmol) in 5 mL of dry dichloromethane was added dropwise over a period of 10 min. The resulting mixture was stirred from 0°C to room temperature for 12 hours. After this time, the reaction was quenched with saturated Na_2CO_3 aqueous solution at 0°C and the product was extracted with dichloromethane. The organic phase was washed with aqueous NH_4Cl, then dried over anhydrous Na_2SO_4 and the solvent evaporated. The residue was purified by silica gel flash chromatography using a mixture of dichloromethane/methanol (99:1) to give product **1** in 50% yield (70 mg).^{1}H NMR ($CDCl_3$, 300 MHz) δ 7.65 (bs, 1H), 7.61 (bs, 3H), 7.56-7.45 (m, 6H), 7.43-7.36 (m, 2H). ^{13}C NMR ($CDCl_3$, 75 MHz) δ 169.0 (C), 166.8 (C), 138.3

(C), 137.3 (C), 130.7 (CH), 129.8 (CH), 129.7 (CH), 129.0 (CH), 128.9 (CH), 128.4 (CH), 127.9 (CH). ESI-MS: 281 $[M+H]^+$.

Synthesis of the Ir(III) complexes

General procedure.

In a 10 ml flask, the desired Ir(III)-dimer (0.025 mmol) (**8–10**) was dissolved in dichloromethane (2 ml) and ethanol (2 drops). $AgBF_4$ (0.05 mmol, 9.8 mg) was added and the solution was stirred for 24 hours in absence of light. Then the formed solid was filtered off and the solution was slowly added to a solution of ligand **4** in dichloromethane (0.05 mmol, 14.5 mg in 13 ml). The resulting mixture was stirred for additional 24 hours. After this time, solvent was evaporated and the crude was purified by flash chromatography on Al_2O_3 using a mixture of dichloromethane/methanol (95:5) to give the expected product.

Complex 2: 25.3 mg, yield = 58%. ^{1}H NMR ($CDCl_3$, 600 MHz, T= -10°C) δ 9.36 (d, *J* = 6 Hz, 1H), 8.12 (t, *J* = 8.4 Hz, 1H), 8.05 (d, *J* = 8.4 Hz, 1H), 7.94-7.90 (m, 2H), 7.88-7.83 (m, 3H), 7.68 (t, *J* = 6.6 Hz, 2H), 7.65-7.60 (m, 2H), 7.56-7.51 (m, 2H), 7.48-7.41 (m, 3H), 7.38 (t, *J* = 7.8 Hz, 1H), 7.34-7.29 (m, 3H), 6.96 (q, *J* = 7.8 Hz, 2H), 6.93 (t, *J* = 7.8 Hz, 1H), 6.88 (t, *J* = 7.8 Hz, 1H), 6.81 (t, *J* = 7.8 Hz, 1H), 6.14 (d, *J* = 7.8 Hz, 1H), 5.99 (d, *J* = 7.8 Hz, 1H). ^{13}C NMR ($CDCl_3$, 150 MHz, T= -10°C) δ 167.0 (C), 166.7 (C), 154.5 (CH), 153.1 (C), 152.0 (C), 151.4 (CH), 143.8 (C), 143.3 (C), 140.3 (C), 139.9 (C), 139.3 (CH), 138.8 (CH), 137.6 (C), 137.0 (C), 132.9 (C), 131.7 (C), 131.1 (CH), 131.0 (CH), 130.9 (CH), 130.8 (CH), 130.7 (CH), 130.6 (CH), 130.4 (CH), 130.3 (CH), 130.2 (CH), 129.7 (CH), 129.3 (CH), 129.2 (CH), 128.9 (CH), 128.8 (CH), 127.2 (CH), 126.4 (CH), 125.2 (CH), 124.6 (CH), 124.5 (CH), 124.1 (C), 123.9 (C), 123.8 (CH), 123.7 (CH), 123.6 (CH), 120.6 (CH), 120.5 (CH). ESI-MS: 781 $(M-BF_4)^+$.

Complex 3: 28.2 mg, yield = 60%. ^{1}H NMR ($CDCl_3$, 600 MHz, T= +25°C) δ 9.55 (d, *J* = 6.0 Hz, 1H), 8.37 (d, *J* = 8.8 Hz, 1H), 8.24 (d, *J* = 7.6 Hz, 1H), 8.08 (t, *J* = 8.0 Hz 1H), 8.06 (t, *J* = 1.6 Hz, 1H), 7.90 (t, *J* = 7.6 Hz, 1H), 7.85 (d, *J* = 6.0 Hz, 1H), 7.81 (t, *J* = 7.6 Hz, 1H), 7.73 (d, *J* = 7.6 Hz, 1H), 7.70 (t, *J* = 6.8 Hz, 1H), 7.65 (d, *J* = 8.0 Hz, 1H), 7.54 (t, *J* = 7.6 Hz, 1H), 7.49-7.42 (m, 3H), 7.40 (t, *J* = 8.0 Hz, 1H), 7.36 (d, *J* = 8.0 Hz, 1H), 7.32 (d, *J* = 7.6 Hz, 1H), 7.29 (d, *J* = 7.6 Hz, 1H), 6.94 (t, *J* = 6.8 Hz, 1H), 6.50-6.42 (m, 2H), 5.59 (dd, *J* = 1.8 Hz, *J* = 8.0 Hz, 1H), 5.42 (dd, *J* = 1.8 Hz, *J* = 8.0 Hz, 1H). ^{13}C NMR ($CDCl_3$, 150 MHz, T= +25°C) δ 164.2 (C, d, *J* = 6.1 Hz), 163.7 (C, dd, J_1 = 257.2 Hz, J_2 = 12.1 Hz), 163.1 (C, d, *J* = 7.2 Hz), 163.4 (C, dd, J_1 = 257.3 Hz, J_2 = 10.8 Hz), 161.4 (C, dd, J_1 = 261.0 Hz, J_2 = 11.5 Hz), 161.3 (C, dd, J_1 = 261.0 Hz, J_2 = 11.5 Hz), 157.0 (C, d, *J* = 6.0 Hz), 156.2 (CH), 155.4 (C, d, *J* = 6.0 Hz), 151.9 (CH), 140.7 (C), 140.1 (C), 140.0 (CH), 139.4 (CH), 138.0 (C), 137.3 (C), 131.3 (C), 131.22 (CH), 131.18 (CH), 130.96 (CH), 130.88 (CH), 130.7 (CH), 130.1 (CH), 129.8 (CH), 129.5 (C), 129.3 (CH), 129.1 (CH), 129.0 (CH), 128.1 (C), 127.9 (CH), 127.4 (C), 126.8 (CH), 126.0 (CH), 124.3 (CH, d, *J* = 21 Hz), 124.1 (CH, d, *J* = 21 Hz), 123.9 (CH), 113.0 (CH, dd, J_1 = 32.8 Hz, J_2 = 18.3 Hz), 100.4 (CH, t, *J* = 26.5 Hz). ^{19}F NMR ($CDCl_3$, 300 MHz, T= +25°C) δ –153.0 (s, 4F), –108.2 (m, 2F), –105.9 (m, 1F), –104.6 (m, 1F). ESI-MS: 853 $(M-BF_4)^+$.

Complex 4: 28.5 mg, yield = 57%. ^{1}H NMR ($CDCl_3$, 600 MHz, T= -10°C) δ 8.67 (d, *J* = 9.0 Hz, 1H), 8.24 (d, *J* = 8.4 Hz, 1H), 8.19 (d, *J* = 8.4 Hz, 1H), 8.09 (d, *J* = 8.4 Hz, 1H), 8.04 (d, *J* = 8.4 Hz, 1H), 7.91 (t, *J* = 7.8 Hz, 1H), 7.82 (t, *J* = 7.8 Hz, 1H), 7.80-7.76 (m, 1H), 7.71 (t, *J* = 7.8 Hz, 1H), 7.63-7.57 (m, 3H), 7.54-7.50

(m,2H), 7.46-7.41 (m,3H), 7.30-7.24 (m, 2H), 7.17 (t, J = 7.8 Hz, 2H), 7.13 (d, J = 7.8 Hz, 2H), 6.98 (t, J = 7.8 Hz, 1H), 6.90 (t, J = 7.8 Hz, 1H), 6.08 (d, J = 7.2 Hz, 1H), 5.87 (d, J = 7.2 Hz, 1H), 3.35 (s, 3H), 3.19 (s, 3H). ^{13}C NMR ($CDCl_3$, 150 MHz, T= -10°C) δ 165.9 (C), 165.4 (C), 155.8 (C), 155.4 (C), 153.1 (C), 152.6 (C), 144.9 (C), 140.6 (C), 140.3 (C), 140.2 (C), 140.1 (C), 139.4 (C), 139.2 (C), 139.7 (C), 136.6 (C), 131.9 (CH), 131.8 (CH), 131.7 (CH), 131.6 (CH), 131.6 (CH), 131.3 (C), 131.3 (CH), 131.2 (CH), 131.1 (C), 131.0 (CH), 130.6 (C), 130.5 (CH), 130.4 (CH), 130.2 (CH), 130.1 (CH), 130.0 (CH), 129.4 (CH), 129.3 (CH), 128.0 (CH), 127.2 (CH), 127.1 (CH), 126.7 (CH), 124.3 (CH), 124.2 (CH), 123.1 (C), 123.0 (C), 27.6 (CH_3). ESI-MS: 911 $(M-BF_4)^+$.

Electrochemistry

Voltammetric experiments were performed using a Metrohm AutoLab PGSTAT 302 electrochemical workstation in combination with the NOVA software package. All the measurements were carried out at room temperature in acetonitrile solutions with a sample concentration approx. 1 mM and using 0.1 M tetrabutylammonium hexafluorophosphate (electrochemical grade, $TBAPF_6$) as supporting electrolyte. Oxygen was removed from the solutions by bubbling argon for 20 minutes. All the experiments were carried out using a three-electrode setup (BioLogic SVC-2 cell, volume range: 5–20 ml) with a platinum disk (1.6 mm diameter) as working electrode, the $Ag/AgNO_3$ redox couple (0.01 M in acetonitrile with 0.1 M $TBAClO_4$ supporting electrolyte) as reference electrode and a platinum wire as counter electrode. At the end of each measurement, ferrocene was added as internal reference. Cyclic voltammograms (CV) were recorded at a scan rate of 100 mV/s (up to 2000 mV/s to check reversibility), while Osteryoung square-wave voltammograms (OSWV) with scan rate of 25 mV/s, a SW amplitude of ±20 mV and a frequency of 25 Hz.

Computational details

Density functional theory (DFT) calculations[27] were carried out using the D.01 revision of the Gaussian 09 program package[28] in combination with the M06 hybrid meta exchange-correlation functional.[17,18] The 6-31G(d,p) basis set was selected for C, H, N and F atoms;[19] on the other hand, the "double-ζ" quality LANL2DZ basis set and the related pseudopotential was adopted for the Ir metal centre.[20] All the complexes were fully optimised, without symmetry constraints, in acetonitrile both in the electronic ground state (S_0) and in the lowest triplet state (T_1) by using the polarisable continuum model (PCM) applying the integral equation formalism model (IEFPCM).[21-23] A frequency calculation was always used to confirm that the stationary point found by the geometry optimisation was actually corresponding to a minimum on the potential energy surface (no imaginary frequencies). Time-dependent DFT calculations (TD-DFT), at the same level of theory used for the geometrical optimisations, were employed to simulate the absorption spectra of all the complexes in their optimized S_0 geometry.[29-31] The first 100 singlet and 25 triplet vertical excitations were computed for the complexes using the non-equilibrium, linear response formalism. To investigate the nature of the T_1 state, geometry optimisations and related frequency calculations were performed at the spin-unrestricted UM06 level of theory, imposing a spin multiplicity of 3. The emission energy from the lowest triplet excited state was estimated by subtracting the SCF energy of the T_1 state in its minimum conformation from that of the singlet ground state having the same geometry of T_1. All the pictures of molecular orbitals and spin-density surfaces were creat-

ed using GaussView 5.[32] The structural overlap of the X-ray crystal structure of **3** and the theoretically computed one is obtained using the VMD program by minimising the root-mean-square deviation (RMSD) of all the atomic positions, except hydrogen.[33]

Photophysical measurements

The spectroscopic investigations were carried out in spectrofluorimetric grade acetonitrile. The absorption spectra were recorded with a Perkin-Elmer Lambda 950 spectrophotometer. For the photoluminescence experiments, the sample solutions were placed in fluorimetric Suprasil quartz cuvettes (1 cm) and dissolved oxygen was removed by bubbling argon for 20 minutes. The uncorrected emission spectra were obtained with an Edinburgh Instruments FLS920 spectrometer equipped with a Peltier-cooled Hamamatsu R928 photomultiplier tube (PMT) (185−850 nm). An Edinburgh Xe 900 (450 W xenon arc lamp) was used as the excitation light source. The corrected spectra were obtained via a calibration curve supplied with the instrument. The photoluminescence quantum yields (Φ_{PL}) in solution were obtained from the corrected spectra on a wavelength scale (nm) and measured according to the approach described by Demas and Crosby[34] using an air-equilibrated water solution of quinine sulfate in 1N H_2SO_4 as reference (Φ_{PL} = 0.546).[35] The emission lifetimes (τ) in the microsecond time range were measured through the time-correlated single photon counting (TCSPC) technique using an HORIBA Jobin Yvon IBH FluoroHub controlling a spectrometer equipped with a pulsed SpectraLED (λ_{exc} = 370 nm; FWHM = 11 nm) as excitation source and a red-sensitive Hamamatsu R-3237-01 PMT (185–850 nm) as detector. The analysis of the luminescence decay profiles was accomplished with the DAS6 Decay Analysis Software provided by the manufacturer, and the quality of the fit was assessed with the χ^2 value close to unity and with the residuals regularly distributed along the time axis. To record the 77 K luminescence spectra, samples were put in quartz tubes (2 mm inner diameter) and inserted into a special quartz Dewar flask filled with liquid nitrogen. Solid samples were prepared by drop casting using a dichloromethane solution containing the poly(methyl methacrylate) (PMMA) matrix with 1% wt. of the complex; the thickness of the films was not controlled. Solid-state Φ_{PL} values were calculated by corrected emission spectra obtained from an Edinburgh FLS920 spectrometer equipped with a barium sulfate-coated integrating sphere (diameter of 4 in.) following the procedure described by Würth *et al*..[36] Experimental uncertainties are estimated to be ±8% for τ determinations, ±20% for Φ_{PL}, ±2 nm and ±5 nm for absorption and emission peaks, respectively.

Acknowledgements

This work was supported by the Italian Ministry of Research (MIUR) (PRIN 2010 INFOCHEM, Contract No. CX2TLM; FIRB Futuro in Ricerca SUPRACARBON, Contract No. RBFR10DAK6) and the Consiglio Nazionale delle Ricerche (CNR) (MACOL PM. P04. 010; Progetto Bandiera N-CHEM).

References

1. R. C. Evans, P. Douglas and C. J. Winscom, *Coord. Chem. Rev.*, 2006, **250**, 2093-2126.

2. L. Flamigni, A. Barbieri, C. Sabatini, B. Ventura and F. Barigelletti, *Top. Curr. Chem.*, 2007, **281**, 143-203.
3. R. D. Costa, E. Orti, H. J. Bolink, F. Monti, G. Accorsi and N. Armaroli, *Angew. Chem. Int. Ed.*, 2012, **51**, 8178-8211.
4. T. Hu, L. He, L. Duan and Y. Qiu, *J. Mater. Chem.*, 2012, **22**, 4206-4215.
5. N. M. Shavaleev, F. Monti, R. D. Costa, R. Scopelliti, H. J. Bolink, E. Orti, G. Accorsi, N. Armaroli, E. Baranoff, M. Gratzel and M. K. Nazeeruddin, *Inorg. Chem.*, 2012, **51**, 2263-2271.
6. N. M. Shavaleev, F. Monti, R. Scopelliti, N. Armaroli, M. Gratzel and M. K. Nazeeruddin, *Organometallics*, 2012, **31**, 6288-6296.
7. N. M. Shavaleev, F. Monti, R. Scopelliti, A. Baschieri, L. Sambri, N. Armaroli, M. Gratzel and M. K. Nazeeruddin, *Organometallics*, 2013, **32**, 460-467.
8. F. Monti, F. Kessler, M. Delgado, J. Frey, F. Bazzanini, G. Accorsi, N. Armaroli, H. J. Bolink, E. Orti, R. Scopelliti, M. K. Nazeeruddin and E. Baranoff, *Inorg. Chem.*, 2013, **52**, 10292-10305.
9. F. Monti, A. Baschieri, I. Gualandi, J. J. Serrano-Perez, J. M. Junquera-Hernandez, D. Tonelli, A. Mazzanti, S. Muzzioli, S. Stagni, C. Roldan-Carmona, A. Pertegas, H. J. Bolink, E. Orti, L. Sambri and N. Armaroli, *Inorg. Chem.*, 2014, **53**, 7709-7721.
10. K. Dedeian, J. M. Shi, E. Forsythe, D. C. Morton and P. Y. Zavalij, *Inorg. Chem.*, 2007, **46**, 1603-1611.
11. X. H. Wang, J. A. Li, M. E. Thompson and J. I. Zink, *J. Phys. Chem. A*, 2007, **111**, 3256-3262.
12. J. Li, P. I. Djurovich, B. D. Alleyne, M. Yousufuddin, N. N. Ho, J. C. Thomas, J. C. Peters, R. Bau and M. E. Thompson, *Inorg. Chem.*, 2005, **44**, 1713-1727.
13. C. Wu, H. F. Chen, K. T. Wong and M. E. Thompson, *J. Am. Chem. Soc.*, 2010, **132**, 3133-3139.
14. M. Nonoyama, *Bull. Chem. Soc. Jpn.*, 1974, **47**, 767-768.
15. S. Sprouse, K. A. King, P. J. Spellane and R. J. Watts, *J. Am. Chem. Soc.*, 1984, **106**, 6647-6653.
16. B. Schmid, F. O. Garces and R. J. Watts, *Inorg. Chem.*, 1994, **33**, 9-14.
17. Y. Zhao and D. G. Truhlar, *Theor. Chem. Acc.*, 2008, **120**, 215-241.
18. Y. Zhao and D. G. Truhlar, *Acc. Chem. Res.*, 2008, **41**, 157-167.
19. M. M. Francl, W. J. Pietro, W. J. Hehre, J. S. Binkley, M. S. Gordon, D. J. Defrees and J. A. Pople, *J. Chem. Phys.*, 1982, **77**, 3654-3665.
20. P. J. Hay and W. R. Wadt, *J. Chem. Phys.*, 1985, **82**, 299-310.
21. J. Tomasi and M. Persico, *Chem. Rev.*, 1994, **94**, 2027-2094.
22. J. Tomasi, B. Mennucci and R. Cammi, *Chem. Rev.*, 2005, **105**, 2999-3093.
23. C. J. Cramer and D. G. Truhlar, in *Solvent Effects and Chemical Reactivity*, eds. O. Tapia and J. Bertrán, Springer Netherlands, 2002, vol. 17, pp. 1-80.
24. E. C. Constable, M. Neuburger, P. Rosel, G. E. Schneider, J. A. Zampese, C. E. Housecroft, F. Monti, N. Armaroli, R. D. Costa and E. Orti, *Inorg. Chem.*, 2013, **52**, 885-897.
25. H. J. Bolink, E. Coronado, R. D. Costa, N. Lardies and E. Orti, *Inorg. Chem.*, 2008, **47**, 9149-9151.
26. C. Poriel, R. Metivier, J. Rault-Berthelot, D. Thirion, F. Barriere and O. Jeannin, *Chem. Commun.*, 2011, **47**, 11703-11705.
27. R. G. Parr and W. Yang, *Density Functional Theory of Atoms and Molecules*, Oxford University Press, Oxford, U.K., 1989.
28. M. J. Frisch, G. W. Trucks, H. B. Schlegel, G. E. Scuseria, M. A. Robb, J. R. Cheeseman, G. Scalmani, V. Barone, B. Mennucci, G. A. Petersson, H. Nakatsuji, M. Caricato, X. Li, H. P.

Hratchian, A. F. Izmaylov, J. Bloino, G. Zheng, J. L. Sonnenberg, M. Hada, M. Ehara, K. Toyota, R. Fukuda, J. Hasegawa, M. Ishida, T. Nakajima, Y. Honda, O. Kitao, H. Nakai, T. Vreven, J. A. Montgomery Jr., J. E. Peralta, F. Ogliaro, M. J. Bearpark, J. Heyd, E. N. Brothers, K. N. Kudin, V. N. Staroverov, R. Kobayashi, J. Normand, K. Raghavachari, A. P. Rendell, J. C. Burant, S. S. Iyengar, J. Tomasi, M. Cossi, N. Rega, N. J. Millam, M. Klene, J. E. Knox, J. B. Cross, V. Bakken, C. Adamo, J. Jaramillo, R. Gomperts, R. E. Stratmann, O. Yazyev, A. J. Austin, R. Cammi, C. Pomelli, J. W. Ochterski, R. L. Martin, K. Morokuma, V. G. Zakrzewski, G. A. Voth, P. Salvador, J. J. Dannenberg, S. Dapprich, A. D. Daniels, O. Farkas, J. B. Foresman, J. V. Ortiz, J. Cioslowski and D. J. Fox, *Gaussian 09, Revision D.01*, (2009) Gaussian, Inc., Wallingford, CT, USA.

29. R. E. Stratmann, G. E. Scuseria and M. J. Frisch, *J. Chem. Phys.*, 1998, **109**, 8218-8224.
30. M. E. Casida, C. Jamorski, K. C. Casida and D. R. Salahub, *J. Chem. Phys.*, 1998, **108**, 4439-4449.
31. R. Bauernschmitt and R. Ahlrichs, *Chem. Phys. Lett.*, 1996, **256**, 454-464.
32. R. Dennington, T. Keith and J. Millam, *GaussView, Version 5*, (2009) Semichem Inc., Shawnee Mission, KS, USA.
33. W. Humphrey, A. Dalke and K. Schulten, *J. Mol. Graphics Modell.*, 1996, **14**, 33-38.
34. G. A. Crosby and J. N. Demas, *J. Phys. Chem.*, 1971, **75**, 991-1024.
35. S. R. Meech and D. Phillips, *J. Photochem.*, 1983, **23**, 193-217.
36. C. Wurth, M. Grabolle, J. Pauli, M. Spieles and U. Resch-Genger, *Nat. Protoc.*, 2013, **8**, 1535-1550.